

Particle sizing in the Mie scattering region: singular-value analysis

S Arridge, P van der Zee, D T Delpy and M Cope

Department of Medical Physics and BioEngineering, University College London, Shropshire House, 11-20 Capper Street, London WC1E 6JA, UK

Received 15 May 1989

Abstract. A method for finding the singular system of the Mie scattering kernel for continuous data over all angles is given, based on a result for the spherical harmonic expansion of the kernel. This technique provides a limit to the system obtained using discrete data. Results are given for continuous data and finite support. A comparison is made with the Fraunhofer kernel as the large-particle limit of the Mie case. The use of weighted spaces for the inversion is discussed.

1. Introduction

The problem of particle size determination by the inversion of a scattered-light distribution has a considerable literature. The description of light scattering from particles admits of three regions:

- (1.i) particles of radius \ll wavelength (Rayleigh scattering);
- (1.ii) particles of radius comparable to the wavelength (Mie scattering);
- (1.iii) particles of radius \gg wavelength (Fraunhofer diffraction limit).

The exact theory for scattering by a spherical particle is solvable from Maxwell's equations [1-3]. The Rayleigh limit can be derived from the small-particle limit to this theory. The Fraunhofer limit is essentially different, however, derived correctly only for small angles in the forward direction, where the approximation $\sin(\theta) \simeq \theta$ is accurate.

In this Fraunhofer region, applicable for radii greater than about ten times the wavelength of light, the scattered intensity $I_s(\theta)$ per unit area of detector, for an incident intensity I_i is given by:

$$I_s(\theta) = g(\theta)I_i = \int_{\alpha_0}^{\alpha_1} |\mathcal{S}(\theta, \alpha)|^2 f(\alpha) d\alpha I_i \quad 0 \leq \theta \leq \pi/2 \quad (1.1)$$

where $f(\alpha)$ is a continuous probability distribution for the particle size parameter $\alpha = 2\pi r n_m / \lambda$ for a particle of radius r and monochromatic radiation of wavelength λ , in a medium of refractive index n_m . $\mathcal{S}(\theta, \alpha)$ is given by

$$\mathcal{S}(\theta, \alpha) = \alpha^2 \frac{1}{2} (1 + \cos(\theta)) \frac{J_1(\alpha \sin(\theta))}{\alpha \sin(\theta)}. \quad (1.2)$$

The singular-value analysis of this case has been fully developed by Bertero *et al* [4, 5]. In their analysis the distribution to be found is in fact $p(\alpha) = \alpha^4 f(\alpha)$ so that the kernel

analysed is

$$\mathcal{H}[p](s) = \int_{\alpha_0}^{\alpha_1} \mathcal{H}(\alpha s) p(\alpha) d\alpha \quad 0 \leq \theta \leq \pi/2 \quad (1.3)$$

with $s = \sin(\theta)$ and

$$\mathcal{H}(z) = (J_1(z)/z)^2. \quad (1.4)$$

This is justifiable since, for the extremely forward-peaked diffraction pattern, the Kirchhoff correction $\frac{1}{2}(1 + \cos(\theta))$ in (1.2) is almost unity over all contributing angles.

Then since (1.4) is of 'product kernel' type [6], the Mellin transform may be employed to develop the singular system of (1.3) in the limit of continuous data and infinite support. In contrast the Mie region presents some complications that, for the scattering kernel, preclude a straightforward analytical solution.

The general method of inversion by finding the eigenvectors of a quadrature matrix approximation to the Mie kernel was introduced by Twomey and Howell [7], and was based on a general method for Fredholm linear equations of the first kind [8, 9]. A number of refined methods have since been developed [10–17]. All authors have noted the attendant errors resulting from quadrature. However, almost all applications have been to aerosol determination from remote-sensing experiments and have considered small-angle ranges either in the forward or backscattered directions, or around another fixed angle. Further, since all workers have noted a considerable ill-conditioning of this kernel, there is always an attempt to incorporate as much *a priori* information as possible about the expected nature of the aerosol size distributions.

Our application is substantially different. We wish to develop a phantom, composed of a mixture of spherical particles, that approximates the angular scattering phase function of light in tissue as measured by a goniometer experiment. We have no *a priori* information apart from an expected upper limit to particle size, but we can effectively use a full angular range.

In this paper, assuming a form like (1.1) for the Mie region we develop the singular system of the Mie scattering kernel for the case of continuous data and finite support, by using a new result for the angular integration of the kernel. Results for some ranges of support are given, and comparison made with the case for discrete data and finite support. A comparison is also made to the Fraunhofer approximation.

The principal new result is that by using the full angular range for the data (i.e. θ in $[0, \pi]$), the kernel may be expanded in spherical harmonics and certain simplifications occur. This treatment is applicable to laboratory-based experiments where a sample or detector may be rotated through all angles.

2. Formulation of the problem

Considering Mie theory, a plane wave may be characterised by the Stokes parameters, $\{I, Q, U, V\}$ [3], where I represents total intensity, Q and U are components of linear polarisation and V of circular polarisation. Then the characteristics of the light scattered by the sphere are given by the relation

$$\begin{pmatrix} I_s \\ Q_s \\ U_s \\ V_s \end{pmatrix} = \frac{1}{\alpha^2} \begin{pmatrix} S_{11} & S_{12} & 0 & 0 \\ S_{12} & S_{11} & 0 & 0 \\ 0 & 0 & S_{33} & S_{34} \\ 0 & 0 & -S_{34} & S_{33} \end{pmatrix} \begin{pmatrix} I_i \\ Q_i \\ U_i \\ V_i \end{pmatrix}. \quad (2.1)$$

The four independent factors S_{11} , S_{12} , S_{33} , and S_{34} are derivable exactly from Maxwell's equations, and are functions of θ , the angle of measurement from the scattering plane, with the problem possessing azimuthal symmetry by definition.

More complex situations may be analysed by constructing an amplitude scattering matrix that is a linear sum of the matrices \mathbf{S} of equation (2.1) for the different particle sizes and refractive indices. Thus, consider the situation where a mixture of particles is irradiated by a plane wave and observed in the far field, where the following assumptions are required:

(2.i) only single-scattering occurs, and no phase relations exist between light scattered from different particles;

(2.ii) the particles are all spheres whereas they may be irregular.

Let the particles have a size distribution $f(\alpha)$ and refractive index distribution $\eta(m)$ where m is the (complex) refractive index. Then we may form the amplitude scattering matrix of the ensemble to obtain

$$I_s(\theta, \lambda) = g(\theta, \lambda)I_i = \int \mathbf{S}(m, \alpha, \theta, \lambda) f(\alpha) \eta(m) \, d\alpha \, dm \, I_i. \tag{2.2}$$

The inverse problem to this is to obtain information about the size and refractive index distribution comprising the linear sum of amplitude scattering matrices. Since, as will be shown, the problem is severely ill-conditioned it is usual to impose a third restriction:

(2.iii) The particles are restricted to only one refractive index (i.e. $\eta(m)$ is a δ -function).

Assumptions (2.i) and (2.ii) are required in order that Mie theory is applicable. Assumption (2.iii) is applicable in some physical applications—for example, the remote sensing of radiation scattered from atmospheric aerosols—but in general need not be accurate.

In most physical applications, measurements are only made of total intensity wherein the incident radiation has $Q_i = U_i = V_i = 0$. In fact if the incident wave is plane polarised then U_s and V_s will still be zero and because of the block diagonal nature of \mathbf{S} in (2.1) only two perpendicular polarisation measurements need be made. Considering the total received intensity, in all cases, equation (2.2) reduces to a Fredholm integral equation of the first kind

$$I_s(\theta, \lambda) = g(\theta, \lambda)I_i = \int \mathcal{K}_m(\alpha, \theta, \lambda) f(\alpha) \, d\alpha \tag{2.3}$$

where I_s and I_i are now scalars, and we have used \mathcal{K}_m to represent the kernel which will depend on the exact measurements being made. In practice, a noise term should also be included.

Two separate possibilities exist for applying the Mie kernel to particle sizing:

Extinction $g(\lambda) = \int_{\alpha_0}^{\alpha_1} \mathcal{K}_m^{(E)}(\alpha, \lambda) f(\alpha) \, d\alpha \tag{2.4}$

Scattering $g(\theta) = \int_{\alpha_0}^{\alpha_1} \mathcal{K}_m^{(S)}(\alpha, \theta) f(\alpha) \, d\alpha. \tag{2.5}$

Formally some other possibilities exist, for example refractive index determination, but these would appear to have less practical applications.

As is well known the inversion of a Fredholm integral equation of the first kind is in general an ill-posed problem, so that an attempted inversion must analyse the nature

of the ill-conditioning of the kernel [8, 9, 18–20]. It is characteristic of naive inversions of Fredholm integrals that oscillations develop in the solution, leading to the use of regularisation techniques.

Naturally it is attractive to analyse this problem analytically as far as is possible. McWhirter and Pike [6] have demonstrated an analytical technique for deriving singular functions and singular values of any kernel of product type

$$\mathcal{K}(x, y) = \mathcal{K}(z) \tag{2.6}$$

where $z = xy$, by use of the Mellin transform, subject to a normalisation criterion that the kernel $\int_0^\infty \mathcal{K} z^{-1/2} dz$ be finite, which is often satisfied by physical kernels. Thus Bertero and Pike [4] have derived the singular spectrum of the Fraunhofer scattering kernel. This analytic technique applies to *continuous* data and infinite support, and has further been shown to give an upper bound to the spectrum for *discrete* data and infinite support. Further investigation of varied bounded and profiled supports is also possible [5].

For the extinction problem the kernel may be written as a function of kr where $k = 2\pi/\lambda$, so that this kernel also falls into the class covered by McWhirter and Pike (equation (2.6)). Viera and Box [21] have obtained the analytic singular functions for this case. Consideration of the Mie scattering kernel is considerably more complex.

2.1. Derivation of the kernel

The derivation of the Mie kernel is well known and need not be given here [1–3]. It is most conveniently found by considering the radial component of the Poynting vector of the scattered radiation from a sphere. An incident plane wave $\mathbf{E}_i \exp[i(\omega t - \mathbf{k} \cdot \mathbf{r})]$ gives rise to internal and scattered waves \mathbf{E}_{int} and \mathbf{E}_s . By expansion in spherical harmonics and matching of boundary conditions at the surface of the sphere, the scattered wave is found to be a superposition of functions whose radial components are Hankel functions, and whose angular components are derived from the associated Legendre polynomials. Using

$$\pi_j(\cos(\theta)) = \frac{P_j^1(\cos(\theta))}{\sin(\theta)} \tag{2.7}$$

$$\tau_j(\cos(\theta)) = \frac{d}{d\theta} P_j^1(\cos(\theta)) \tag{2.8}$$

where $P_j^1(\mu)$ is the associated Legendre polynomial of order j and degree 1, the Poynting vector is derived as $(\mathbf{E} \wedge \mathbf{H})$ and its radial component gives rise to

$$\begin{aligned} \mathcal{K}(\mu, \alpha) = & \sum_{n,m} \frac{(2n+1)(2m+1)}{n(n+1)m(m+1)} \\ & \times [(a_n(\alpha)a_m(\alpha) + b_n(\alpha)b_m(\alpha))(\pi_n(\mu)\pi_m(\mu) + \tau_n(\mu)\tau_m(\mu)) \\ & + (a_n(\alpha)b_m(\alpha) + b_n(\alpha)a_m(\alpha))(\pi_n(\mu)\tau_m(\mu) + \tau_n(\mu)\pi_m(\mu))] \end{aligned} \tag{2.9}$$

where $\mu = \cos(\theta)$ and

$$a_j = \frac{v\psi_j(vx)\psi'_j(x) - \psi_j(x)\psi'_j(vx)}{v\psi_j(vx)\zeta'_j(x) - \zeta_j(x)\psi'_j(vx)} \tag{2.10}$$

$$b_j = \frac{\psi_j(vx)\psi'_j(x) - v\psi_j(x)\psi'_j(vx)}{\psi_j(vx)\zeta'_j(x) - v\zeta_j(x)\psi'_j(vx)} \tag{2.11}$$

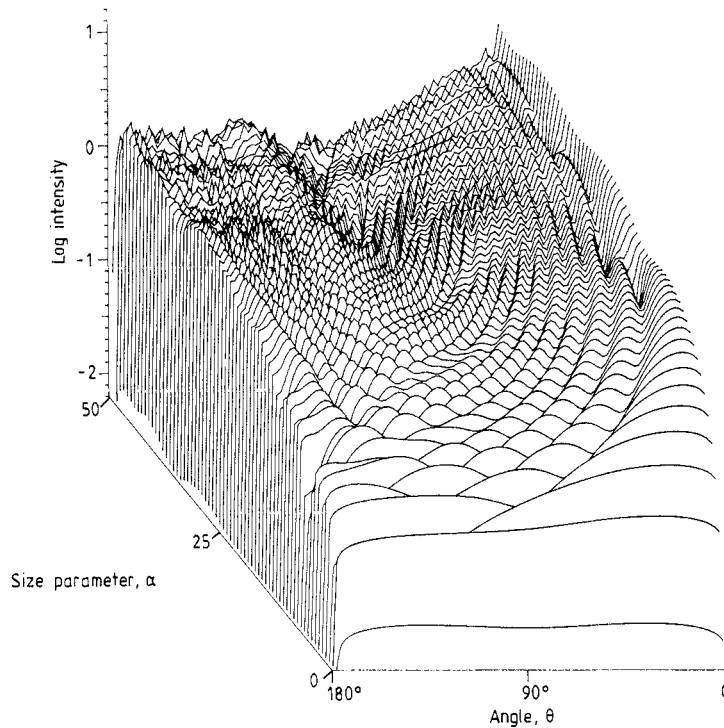


Figure 1. An isometric plot of the log intensity (arbitrary units) of the Mie scattering kernel. The horizontal axis plots angle θ from 0 to 180° and the oblique axis plots size parameter α from 0 to 50.

$\psi_k(x) = xj_k(x)$ and $\xi_k(x) = xh_k^{(1)}(x)$ are the Ricatti-Bessel functions, j_k the spherical Bessel function of order k , and $h_k^{(1)}$ the Hankel function (spherical Bessel function of the third kind). Here $\nu = n_p/n_m$ is the relative refractive index of particle and medium.

The inversion of the Mie kernel is potentially interesting because the kernel itself possesses a high degree of oscillation which suggests that the classic instability due to the smoothing out of fast oscillatory components in the solution space may not occur. However, in practice the oscillation of the kernel is so fine that the particle distribution would need to be computed on an extremely fine quadrature grid. This itself produces attendant problems with the noise in the data.

Figure 1 indicates the behaviour of the Mie kernel. The log intensity has been plotted as a function of α from 0 to 50 and of θ from 0 to 180 degrees, for a relative refractive index of 1.2 (no imaginary component). The precise nature of the oscillation has been studied carefully. Fahlen and Bryant [22] report that the principal oscillation is at $2(m - 1)$ in α , where m is the real part of m , and is explicable in terms of surface waves on the sphere. Other oscillations are at 0.8 and 0.277 in α . It has been stated that ripple structure does not exist below 10^{-7} in α [23], but this is far too fine an interval to use in the construction of a matrix approximation to the kernel.

2.2. Definition of the operator interpretation of the Mie kernel

In the following we consider the Mie kernel as an operator from $L^2[\alpha_0, \alpha_1]$ to $L^2[-1, 1]$. We will include a discussion of weighted spaces for comparison with the Fraunhofer

case [5]. Thus define the integral operator under consideration as

$$g(\mu) = \mathcal{K}[f; P](\mu) = \int_{\alpha_0}^{\alpha_1} \frac{\mathcal{K}(\mu, \alpha)}{P(\alpha)} f(\alpha) P(\alpha) d\alpha \quad -1 \leq \mu \leq 1 \quad (2.12)$$

with \mathcal{K} given by equation (2.9), and the profiling factor $P(\alpha)$ introduced to allow weighted inversions. Unless explicitly stated, the profiling function is 1. Bertero *et al* [4, 5] choose to scale the variables $x = \alpha_0 \mu$ and $y = \alpha/\alpha_0$ so that the integral (2.12) is always $[1, \gamma]$ where $\gamma = \alpha_1/\alpha_0$. We refer to this parameter later in the comparison to the Fraunhofer case.

3. Continuous data and finite support

We assume that the intensity function $g(\mu)$ is given on all μ in $[\mu_0, \mu_1]$. Then the inversion of equation (2.12) is equivalent to finding the inverse operator to \mathcal{K} . The singular system $\{\sigma_k; u_k, v_k\}$ is defined by:

$$\sigma_k v_k(\mu) = \mathcal{K}[u_k(\alpha)] \quad (3.1)$$

$$\sigma_k u_k(\alpha) = \mathcal{K}^*[v_k(\mu)] \quad (3.2)$$

where the adjoint operator \mathcal{K}^* is given by

$$\mathcal{K}^*[g](\alpha) = \int_{\mu_0}^{\mu_1} \mathcal{K}(\mu, \alpha) g(\mu) d\mu \quad (3.3)$$

and the generalised inverse is \mathcal{K}^\dagger given by

$$\mathcal{K}^\dagger[g](\alpha) = (\mathcal{K}^* \mathcal{K})^{-1} \mathcal{K}^*[g]. \quad (3.4)$$

Then the singular functions $u_k(\alpha)$ are the eigenfunctions associated with eigenvalues $c_k = \sigma_k^2$, of the self-adjoint, positive definite integral operator

$$\mathcal{K}^* \mathcal{K}[u_k](\alpha) = \int_{\alpha_0}^{\alpha_1} \mathcal{B}(\alpha, \alpha') u_k(\alpha') d\alpha' = c_k u_k(\alpha) \quad \alpha_0 \leq \alpha \leq \alpha_1 \quad (3.5)$$

where $\mathcal{B}(\alpha, \alpha')$ is given by

$$\mathcal{B}(\alpha, \alpha') = \int_{\mu_0}^{\mu_1} \mathcal{K}(\mu, \alpha) \mathcal{K}(\mu, \alpha') d\mu \quad \alpha_0 \leq \alpha \leq \alpha_1 \quad (3.6)$$

and similarly

$$\mathcal{K} \mathcal{K}^*[v_k](\mu) = \int_{\mu_0}^{\mu_1} \mathcal{C}(\mu, \mu') v_k(\mu') d\mu' = c_k v_k(\mu) \quad \mu_0 \leq \mu \leq \mu_1 \quad (3.7)$$

where $\mathcal{C}(\mu, \mu')$ is given by

$$\mathcal{C}(\mu, \mu') = \int_{\alpha_0}^{\alpha_1} \mathcal{K}(\mu, \alpha) \mathcal{K}(\mu', \alpha) d\alpha \quad \mu_0 \leq \mu \leq \mu_1. \quad (3.8)$$

Consider the form of $\mathcal{B}(\alpha, \alpha')$ in the limit of full angular data, i.e. $[\mu_0, \mu_1] \rightarrow [-1, 1]$. We make use of the convolution theorem for the Legendre transform [24] to write:

$$\mathcal{B}(\alpha, \alpha') = \sum_{j=0}^{\infty} (j + \frac{1}{2}) \bar{K}_L(j, \alpha) \bar{K}_L(j, \alpha') \quad (3.9)$$

where the Legendre transform of a function $f(\mu)$ is defined by:

$$\tilde{f}_L(j) = \int_{-1}^1 P_j^0(\mu) f(\mu) d\mu. \tag{3.10}$$

In a previous paper [25] we determined the Legendre transform of the Mie kernel as

$$\begin{aligned} \tilde{K}_L(j, \alpha) = \frac{1}{2\alpha^2} \sum_{n,m}^{N_{\max}} \frac{(2n+1)(2m+1)}{\lambda_n \lambda_m} \{ A_{m,n} \frac{1}{2} [\lambda_j - (\lambda_n + \lambda_m)] (\lambda_m \lambda_j)^{1/2} \\ \times C(j, m, n; 1, 1, -1) C(j, m, n; 0, 0, 0) - B_{m,n} Z \} \end{aligned} \tag{3.11}$$

where

$$Z = \begin{cases} \sum_{k=0}^{(j-1)/2} (4k+1) (\lambda_m \lambda_{2k})^{1/2} C(2k, m, n; 1, 1, -1) C(2k, m, n; 0, 0, 0) & j \text{ odd} \\ \sum_{k=0}^{j/2-1} (4k+3) (\lambda_m \lambda_{2k+1})^{1/2} C(2k+1, m, n; 1, 1, -1) C(2k+1, m, n; 0, 0, 0) & j \text{ even} \end{cases}$$

and $A_{n,m}$ and $B_{n,m}$ are defined in terms of the Mie coefficients (2.10) and (2.11) as

$$A_{n,m}(\alpha) = a_n(\alpha) a_m(\alpha) + b_n(\alpha) b_m(\alpha) \tag{3.12}$$

$$B_{n,m}(\alpha) = a_n(\alpha) b_m(\alpha) + b_n(\alpha) a_m(\alpha) \tag{3.13}$$

and where $\lambda_j = -j(j+1)$ and N_{\max} is the maximum term in the summation for the Mie kernel. The terms $C(i, j, k; m, n, p)$ are the Clebsh–Gordan coefficients [26, 27]. The method is summarised in the appendix. We thus have an exact form for the operator \mathcal{B} for any α, α' , and the σ_k and u_k can be obtained by eigen decomposition of its symmetric matrix representation.

Derivation of the data space singular vectors $v_k(\mu)$ on the other hand will require numerical integration of the operator $\mathcal{C}(\mu, \mu')$. Thus \mathcal{C} must be derived from a summation of the form

$$\mathcal{C}^{(M)}(\mu, \mu') = \sum_{m=1}^M \delta_m \mathcal{K}(\mu, \alpha_m) \mathcal{K}(\mu', \alpha_m) \tag{3.14}$$

where δ_m is the quadrature weight. Because of the oscillatory nature of \mathcal{K} as a function of α , this will be very sensitive to the quadrature used. A better method therefore is to use equation (3.1) directly.

4. Discrete data and finite support

We now assume that the function $g(\mu)$ is given only on a finite set of points $\{\zeta_1, \zeta_2, \dots, \zeta_N\}$ so that equation (2.12) is now

$$g(\zeta_n) = \mathcal{K}_N[f; P](\zeta_n) = \int_{\alpha_0}^{\alpha_1} \frac{\mathcal{K}(\zeta_n, \alpha)}{P(\alpha)} f(\alpha) P(\alpha) d\alpha \quad n = 1, \dots, N \tag{4.1}$$

and the norm in the space of the data is given by a scalar product such as

$$(g_1, g_2) = \sum_{n=1}^N w_n g_1(\zeta_n) g_2(\zeta_n) \quad (4.2)$$

with the weights w_n introduced for the quadrature integration. It is precisely here that care must be taken because of the very oscillatory nature of the kernel.

The adjoint operator \mathcal{K} is given by

$$\mathcal{K}_N^*[g](\alpha) = \sum_{n=1}^N w_n \mathcal{K}(\zeta_n, \alpha) g(\zeta_n) \quad \alpha_0 \leq \alpha \leq \alpha_1. \quad (4.3)$$

Then the singular functions $u_{N,k}(\alpha)$ are the eigenfunctions associated with eigenvalues $c_{N,k} = \sigma_{N,k}^2$, of the self-adjoint, positive definite integral operator

$$\mathcal{K}_N^* \mathcal{K}_N[u_{N,k}](\alpha) = \int_{\alpha_0}^{\alpha_1} \mathcal{B}_N(\alpha, \alpha') u_{N,k}(\alpha') d\alpha' = c_{N,k} u_{N,k}(\alpha) \quad \alpha_0 \leq \alpha \leq \alpha_1 \quad (4.4)$$

where $\mathcal{B}_N(\alpha, \alpha')$ is given by

$$\mathcal{B}_N(\alpha, \alpha') = \sum_{n=1}^N w_n \mathcal{K}(\zeta_n, \alpha) \mathcal{K}(\zeta_n, \alpha') \quad \alpha_0 \leq \alpha \leq \alpha_1 \quad (4.5)$$

and similarly

$$\mathcal{K}_N \mathcal{K}_N^*[v_{N,k}](\zeta_m) = \sum_{n=1}^N \mathcal{C}_{n,m}^{(N)} v_{N,k}(\zeta_n) = c_k u_{N,k}(\zeta_m) \quad (4.6)$$

where $\mathcal{C}_{n,m}^{(N)}$ is given by

$$\mathcal{C}_{n,m}^{(N)} = \int_{\alpha_0}^{\alpha_1} \mathcal{K}(\zeta_n, \alpha) \mathcal{K}(\zeta_m, \alpha) d\alpha \quad n, m = 1, \dots, N. \quad (4.7)$$

In addition, as pointed out above, the α integration also requires a quadrature approximation. We thus require eigenvalues of the matrix operator defined by

$$(\mathcal{K}_{N,M}^* \mathcal{K}_{N,M})_{ij} u_{N,k}(\alpha_j) = \sum_{j=1}^M \delta_j \mathcal{B}_{N,M}(\alpha_i, \alpha_j) u_{N,k}(\alpha_j) \quad (4.8)$$

where

$$\mathcal{B}_{N,M}(\alpha_i, \alpha_j) = \sum_{n=1}^N w_n \mathcal{K}(\zeta_n, \alpha_i) \mathcal{K}(\zeta_n, \alpha_j) \quad i, j = 1, \dots, M. \quad (4.9)$$

In the following results we consider equal spacing in θ which leads to $w_n = \sin(\theta_n) d\theta$, and linear spacing in α .

5. Results

We compare results from the methods described in §§ 3 and 4 for the Mie and Fraunhofer cases. The singular spectrum for continuous data was computed by the method of § 3, with unity profiling function, for five different ranges of particle radius (in μm): [0.1–1.0], [0.2–2.0], [0.1–0.5], [0.2–1.0] and [0.4–2.0]. The values $n_m = 1.33$, $n_p = 1.6$, $\lambda = 0.783 \mu\text{m}$ were used in all cases, so the ranges $[\alpha_0 - \alpha_1]$ were, respectively: [1.067–10.67], [2.134–21.34],

Table 1. Comparison of continuous data and quadrature integration data for the first ten singular values of the Mie scattering kernel, with refractive index of medium $n_m = 1.33$, refractive index of particle $n_p = 1.6$, and wavelength of light $\lambda = 0.783 \mu\text{m}$, for five different ranges of size parameter α . The ratio parameter $\gamma(\alpha_1/\alpha_0)$ is either 10 or 5, as indicated for each parameter size range.

No	Continuous	1° quadrature	2° quadrature
$\alpha = [1.067-10.67] \quad \gamma = 10$			
1	$1.250\,974 \times 10^3$	$1.245\,39 \times 10^3$	$1.228\,08 \times 10^3$
2	$2.920\,230 \times 10^2$	$2.909\,12 \times 10^2$	$2.871\,89 \times 10^2$
3	$1.600\,204 \times 10^2$	$1.599\,90 \times 10^2$	$1.598\,94 \times 10^2$
4	$1.251\,236 \times 10^2$	$1.248\,83 \times 10^2$	$1.240\,10 \times 10^2$
5	$4.563\,135 \times 10$	$4.559\,93 \times 10$	$4.548\,09 \times 10$
6	$4.217\,968 \times 10$	$4.216\,63 \times 10$	$4.211\,78 \times 10$
7	$1.845\,691 \times 10$	$1.845\,30 \times 10$	$1.843\,76 \times 10$
8	$1.556\,203 \times 10$	$1.555\,80 \times 10$	$1.554\,33 \times 10$
9	8.522 957	8.522 36	8.519 88
10	6.926 007	6.924 73	6.920 12
$\alpha = [2.134-21.34] \quad \gamma = 10$			
1	$3.676\,859 \times 10^2$	$3.672\,27 \times 10^2$	$3.658\,38 \times 10^2$
2	$4.526\,433 \times 10$	$4.522\,24 \times 10$	$4.509\,28 \times 10$
3	$1.287\,337 \times 10$	$1.286\,99 \times 10$	$1.285\,91 \times 10$
4	4.466 705	4.465 62	4.462 20
5	2.004 997	2.004 74	2.003 93
6	1.005 300	1.005 19	1.004 85
7	$5.424\,855 \times 10^{-1}$	$5.424\,53 \times 10^{-1}$	$5.423\,48 \times 10^{-1}$
8	$3.394\,732 \times 10^{-1}$	$3.394\,61 \times 10^{-1}$	$3.394\,21 \times 10^{-1}$
9	$2.118\,331 \times 10^{-1}$	$2.118\,32 \times 10^{-1}$	$2.118\,30 \times 10^{-1}$
10	$1.623\,121 \times 10^{-1}$	$1.623\,11 \times 10^{-1}$	$1.623\,06 \times 10^{-1}$
$\alpha = [1.067-5.336] \quad \gamma = 5$			
1	$1.718\,029 \times 10$	$1.717\,49 \times 10$	$1.715\,85 \times 10$
2	1.601 136	1.600 80	1.599 78
3	$3.155\,225 \times 10^{-1}$	$3.154\,88 \times 10^{-1}$	$3.153\,85 \times 10^{-1}$
4	$8.998\,102 \times 10^{-2}$	$8.997\,62 \times 10^{-2}$	$8.996\,17 \times 10^{-2}$
5	$3.664\,497 \times 10^{-2}$	$3.664\,33 \times 10^{-2}$	$3.663\,84 \times 10^{-2}$
6	$2.005\,072 \times 10^{-2}$	$2.004\,81 \times 10^{-2}$	$2.004\,02 \times 10^{-2}$
7	$1.583\,609 \times 10^{-2}$	$1.583\,59 \times 10^{-2}$	$1.583\,53 \times 10^{-2}$
8	$6.050\,888 \times 10^{-3}$	$6.050\,76 \times 10^{-3}$	$6.050\,39 \times 10^{-3}$
9	$2.502\,858 \times 10^{-3}$	$2.502\,33 \times 10^{-3}$	$2.500\,59 \times 10^{-3}$
10	$9.178\,343 \times 10^{-5}$	$9.175\,19 \times 10^{-5}$	$9.168\,59 \times 10^{-5}$
$\alpha = [2.134-10.67] \quad \gamma = 5$			
1	$3.677\,025 \times 10^2$	$3.672\,43 \times 10^2$	$3.658\,55 \times 10^2$
2	$4.527\,517 \times 10$	$4.523\,32 \times 10$	$4.510\,36 \times 10$
3	$1.288\,040 \times 10$	$1.287\,69 \times 10$	$1.286\,60 \times 10$
4	4.470 581	4.469 49	4.466 07
5	2.007 372	2.007 11	2.006 30
6	1.006 351	1.006 24	1.005 90
7	$5.427\,450 \times 10^{-1}$	$5.427\,12 \times 10^{-1}$	$5.426\,08 \times 10^{-1}$
8	$3.393\,721 \times 10^{-1}$	$3.393\,60 \times 10^{-1}$	$3.393\,20 \times 10^{-1}$
9	$2.108\,685 \times 10^{-1}$	$2.108\,68 \times 10^{-1}$	$2.108\,65 \times 10^{-1}$
10	$1.624\,032 \times 10^{-1}$	$1.624\,02 \times 10^{-1}$	$1.623\,97 \times 10^{-1}$

Table 1. (continued)

No	Continuous	1° quadrature	2° quadrature
$\alpha = [4.269-21.34] \quad \gamma = 5$			
1	$1.251\,358 \times 10^3$	$1.245\,77 \times 10^3$	$1.228\,45 \times 10^3$
2	$2.921\,112 \times 10^2$	$2.909\,99 \times 10^2$	$2.872\,72 \times 10^2$
3	$1.601\,437 \times 10^2$	$1.601\,13 \times 10^2$	$1.600\,17 \times 10^2$
4	$1.251\,330 \times 10^2$	$1.248\,93 \times 10^2$	$1.240\,19 \times 10^2$
5	$4.564\,684 \times 10$	$4.561\,45 \times 10$	$4.549\,49 \times 10$
6	$4.225\,184 \times 10$	$4.223\,86 \times 10$	$4.219\,06 \times 10$
7	$1.842\,755 \times 10$	$1.842\,35 \times 10$	$1.840\,77 \times 10$
8	$1.557\,165 \times 10$	$1.556\,76 \times 10$	$1.555\,29 \times 10$
9	8.468 295	8.467 61	8.464 80
10	6.887 522	6.886 23	6.881 51

[1.067–5.336], [2.134–10.67] and [4.269–21.34]. The values of the first ten singular values are given in column 2 of table 1. These are compared to the results for the same particle ranges computed from quadrature integration on 1° and 2° intervals. The values appear to approach the continuous case from below. The first two intervals have the ratio parameter $\gamma(\alpha_1/\alpha_0) = 10$ and the other three have $\gamma = 5$ but, as opposed to the Fraunhofer case, the results are not independent of α_0 .

In all cases the singular functions obtained with discrete data closely approximated those obtained with continuous data. Some examples are shown in figures 2 and 3. In figures 2(a) and (b) the case of $\gamma = 10$, and $r_0 = 0.2$ ($\alpha_0 = 2.134$) is shown. The first three even vectors in solution space (i.e. v_0, v_2, v_4) are shown in (a) and the first three odd vectors (i.e. v_1, v_3, v_5) in (b). Figures 2(c) and (d) show the corresponding vectors for the case $\gamma = 5$ and the same α_0 (2.134). In figure 3 the corresponding data space vectors for these cases are shown.

It is interesting to test whether the Mie kernel does approach the Fraunhofer limit as $\alpha \rightarrow \infty$. The results for discrete data were compared with those of Bertero *et al* [5] for the cases $\gamma = 5$, and $\gamma = 10$, for $\alpha_0 = 2.134, 21.34, 53.36$ and 213.4 . Their results were reproduced using the kernel defined in equation (1.4), using equal spacing in $\sin(\theta)$ up to the first zero of $J_1(x)$ (24 data points) and the second zero (48 data points), as presented in table 2, column 2.

To compare with the Mie theory, a profile function of $P(\alpha) = \alpha^4$ was employed, so that the operator used was $\mathcal{K}_N[f; \alpha^4]$. The Mie functions were computed for the exact angles corresponding to the samples in the Fraunhofer case, and integrated with a constant quadrature in $\sin(\theta)$. In all cases the α interval was divided into 50 equal intervals (i.e. $M = 50$ in equation (4.8)). The results are given in table 2, columns 3–6, for the four different values of α_0 . Although of the same order of magnitude, there are considerable differences.

6. Decomposition in weighted spaces

Here, an α^4 weighting was employed to make the kernel consistent with Bertero *et al* [5]. In physical terms this technique incorporates some of the solution function into the kernel. In the limit, if the profiling function were the solution, then the derived solution

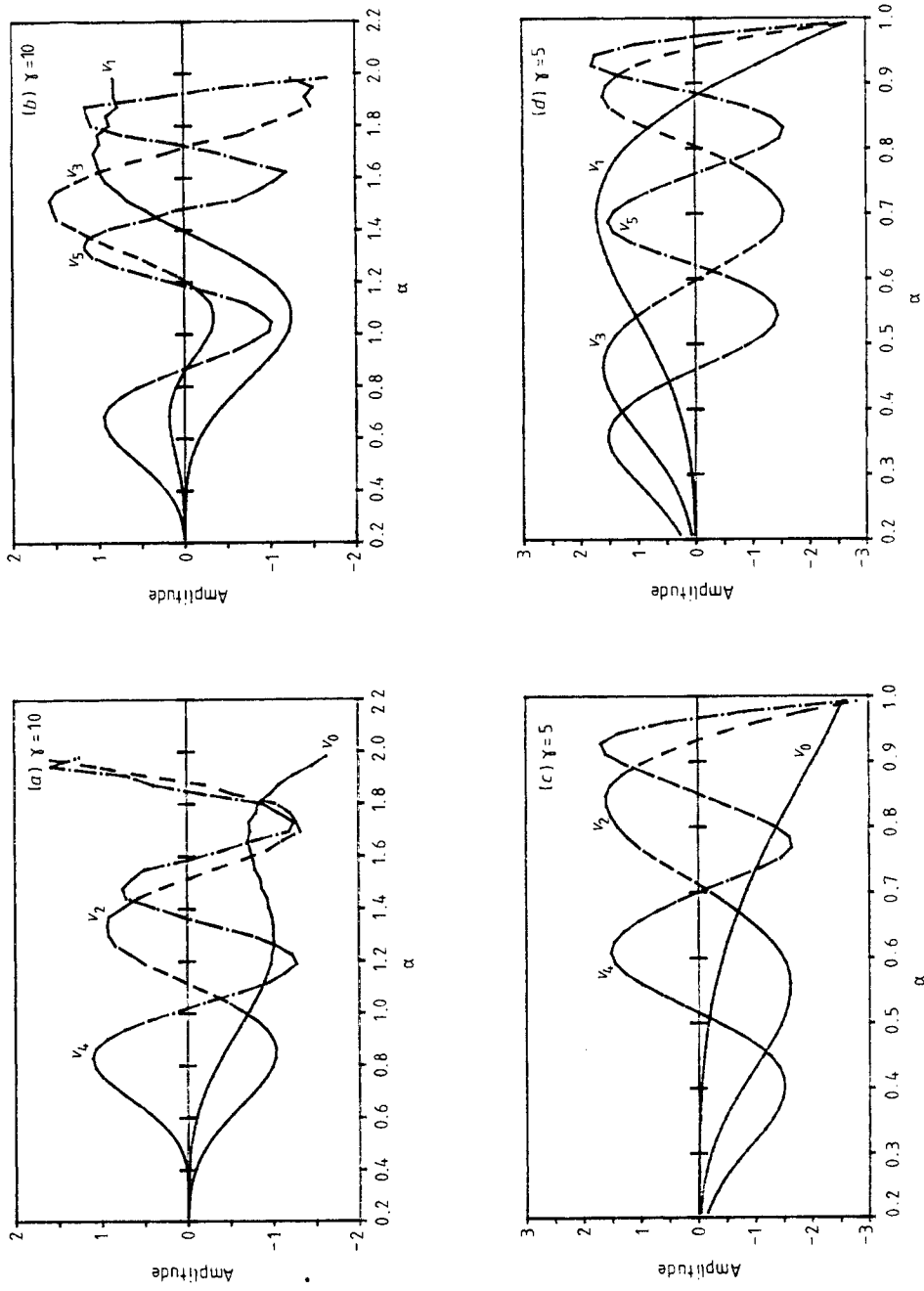


Figure 2. The first six singular vectors v_0, \dots, v_5 in solution space for the Mie kernel with $n_m = 1.33, n_p = 1.6, \lambda = 0.783 \mu\text{m}, \alpha_0 = 2.134$ for (a, b) $\gamma = 10$ and (c, d) $\gamma = 5$. The first three even vectors are shown in (a) and (c) and the first three odd vectors in (b) and (d).

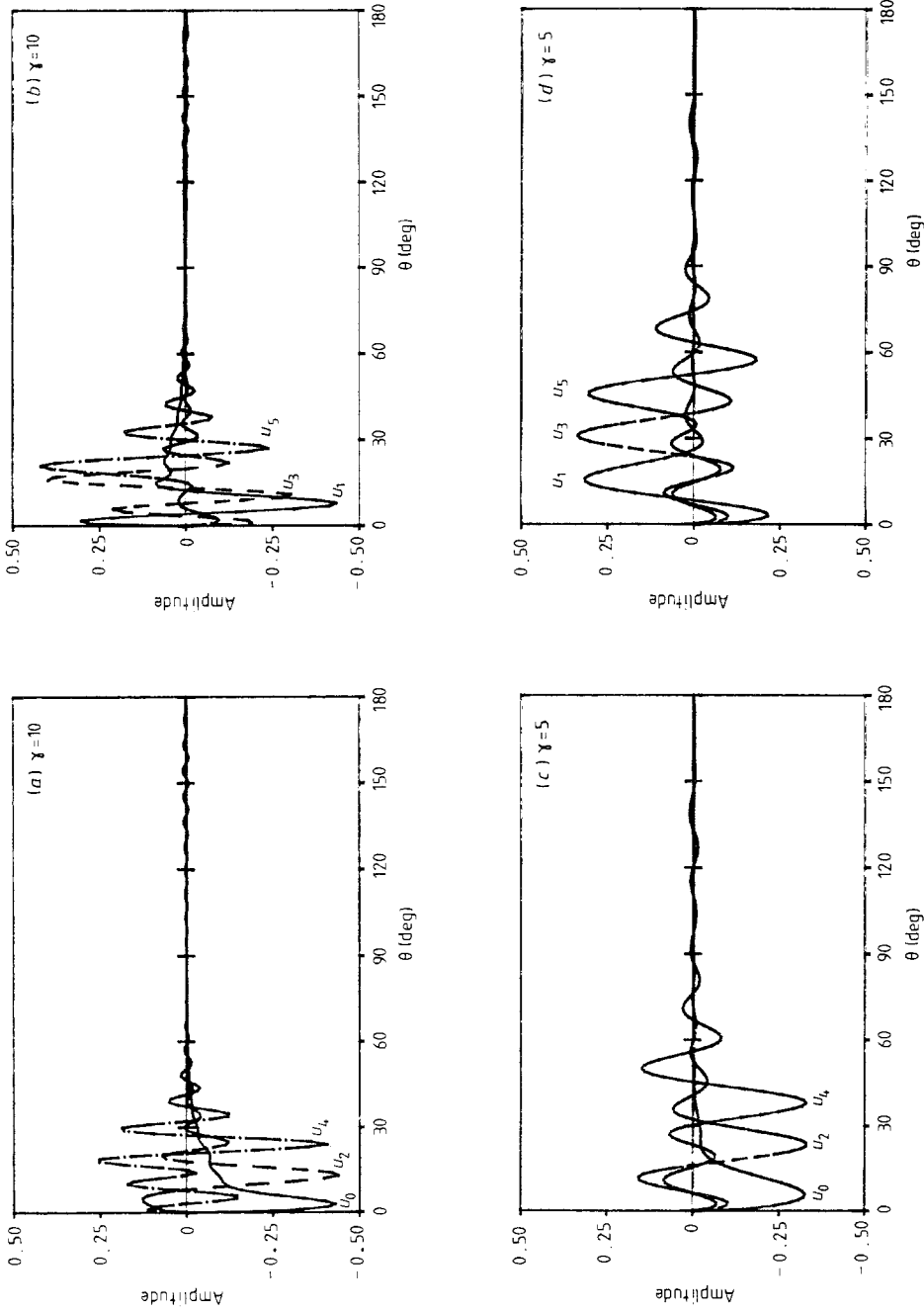


Figure 3. The first six singular vectors u_0, \dots, u_5 in data space for the Mic kernel with $n_m = 1.33$, $n_p = 1.6$, $\lambda = 0.783 \mu\text{m}$, $\alpha_0 = 2.134$ for (a, b) $\gamma = 10$ and (c, d) $\gamma = 5$. The first three even vectors are shown in (a) and (c) and the first three odd vectors in (b) and (d).

Table 2. Comparison of the first ten singular values from the Fraunhofer kernel (for $\gamma = 5$ and 10 and for 24 and 48 data points) with values from the Mie kernel computed at the same angular sample points.

No	Fraunhofer kernel	Mie kernel			
		$\alpha_0 = 2.134$	$\alpha_0 = 21.34$	$\alpha_0 = 53.36$	$\alpha_0 = 213.4$
$\gamma = 5$ 24 data points					
1	3.039×10^{-1}	1.270×10^{-1}	2.104×10^{-1}	2.794×10^{-1}	5.176×10^{-1}
2	9.224×10^{-2}	3.244×10^{-2}	4.852×10^{-2}	6.582×10^{-2}	1.209×10^{-1}
3	3.182×10^{-2}	9.126×10^{-3}	1.378×10^{-2}	1.819×10^{-2}	3.159×10^{-2}
4	1.285×10^{-2}	3.894×10^{-3}	7.163×10^{-3}	6.720×10^{-3}	1.022×10^{-2}
5	5.996×10^{-3}	1.666×10^{-3}	4.472×10^{-3}	3.815×10^{-3}	4.185×10^{-3}
6	3.128×10^{-3}	7.748×10^{-4}	2.235×10^{-3}	3.224×10^{-3}	2.323×10^{-3}
7	1.757×10^{-3}	4.016×10^{-4}	2.051×10^{-3}	1.818×10^{-3}	1.988×10^{-3}
8	1.040×10^{-3}	2.507×10^{-4}	1.356×10^{-3}	1.443×10^{-3}	1.639×10^{-3}
9	6.473×10^{-4}	2.102×10^{-4}	1.076×10^{-3}	1.177×10^{-3}	1.125×10^{-3}
10	4.046×10^{-4}	1.464×10^{-4}	9.061×10^{-4}	9.522×10^{-4}	7.744×10^{-4}
$\gamma = 5$ 48 data points					
1	3.065×10^{-1}	2.289×10^{-1}	3.712×10^{-1}	5.076×10^{-1}	9.498×10^{-1}
2	9.290×10^{-2}	4.640×10^{-2}	1.128×10^{-1}	1.539×10^{-1}	2.864×10^{-1}
3	3.199×10^{-2}	1.546×10^{-2}	3.923×10^{-2}	5.430×10^{-2}	9.958×10^{-2}
4	1.291×10^{-2}	6.003×10^{-3}	1.683×10^{-2}	2.288×10^{-2}	4.057×10^{-2}
5	6.031×10^{-3}	2.593×10^{-3}	1.023×10^{-2}	1.141×10^{-2}	1.913×10^{-2}
6	3.176×10^{-3}	1.220×10^{-3}	7.450×10^{-3}	6.541×10^{-3}	1.019×10^{-2}
7	1.837×10^{-3}	6.158×10^{-4}	4.408×10^{-3}	5.360×10^{-3}	5.978×10^{-3}
8	1.143×10^{-3}	3.283×10^{-4}	3.055×10^{-3}	4.099×10^{-3}	3.824×10^{-3}
9	7.514×10^{-4}	1.910×10^{-4}	2.793×10^{-3}	2.737×10^{-3}	3.129×10^{-3}
10	5.149×10^{-4}	1.354×10^{-4}	2.010×10^{-3}	2.029×10^{-3}	2.563×10^{-3}
$\gamma = 10$ 24 data points					
1	3.318×10^{-1}	1.336×10^{-1}	2.096×10^{-1}	2.790×10^{-1}	5.183×10^{-1}
2	1.261×10^{-1}	3.413×10^{-2}	4.919×10^{-2}	6.605×10^{-2}	1.212×10^{-1}
3	5.315×10^{-2}	1.026×10^{-2}	1.331×10^{-2}	1.831×10^{-2}	3.147×10^{-2}
4	2.491×10^{-2}	4.696×10^{-3}	6.857×10^{-3}	6.874×10^{-3}	9.985×10^{-3}
5	1.290×10^{-2}	2.156×10^{-3}	4.633×10^{-3}	3.792×10^{-3}	3.933×10^{-3}
6	7.278×10^{-3}	1.473×10^{-3}	2.283×10^{-3}	3.259×10^{-3}	2.238×10^{-3}
7	4.407×10^{-3}	7.672×10^{-4}	2.072×10^{-3}	1.854×10^{-3}	1.756×10^{-3}
8	2.820×10^{-3}	3.924×10^{-4}	1.380×10^{-3}	1.593×10^{-3}	1.417×10^{-3}
9	1.879×10^{-3}	2.547×10^{-4}	1.085×10^{-3}	1.118×10^{-3}	8.394×10^{-4}
10	1.293×10^{-3}	2.176×10^{-4}	8.247×10^{-4}	9.537×10^{-4}	6.665×10^{-4}
$\gamma = 10$ 48 data points					
1	3.363×10^{-1}	2.587×10^{-1}	3.806×10^{-1}	5.264×10^{-1}	9.917×10^{-1}
2	1.286×10^{-1}	6.025×10^{-2}	1.294×10^{-1}	1.800×10^{-1}	3.388×10^{-1}
3	5.425×10^{-2}	2.683×10^{-2}	4.942×10^{-2}	6.939×10^{-2}	1.289×10^{-1}
4	2.546×10^{-2}	1.329×10^{-2}	2.107×10^{-2}	3.007×10^{-2}	5.451×10^{-2}
5	1.319×10^{-2}	7.395×10^{-3}	1.108×10^{-2}	1.491×10^{-2}	2.581×10^{-2}
6	7.454×10^{-3}	4.433×10^{-3}	9.000×10^{-3}	8.518×10^{-3}	1.358×10^{-2}
7	4.526×10^{-3}	2.809×10^{-3}	5.733×10^{-3}	5.478×10^{-3}	7.800×10^{-3}
8	2.917×10^{-3}	1.846×10^{-3}	3.521×10^{-3}	5.073×10^{-3}	4.833×10^{-3}
9	1.972×10^{-3}	1.241×10^{-3}	2.993×10^{-3}	3.473×10^{-3}	3.300×10^{-3}
10	1.388×10^{-3}	8.494×10^{-4}	2.438×10^{-3}	2.451×10^{-3}	2.910×10^{-3}

vector would be the unit vector $\mathbf{1}$. The use of profiling functions was suggested by Bertero *et al* [5] because of the need to prevent unnatural truncation at the boundaries of the support. However the use of ‘infinite’ profiling functions is unrealistic because of the time required to compute the Mie kernels.

In figures 4 and 5 are shown the $v_k(\mu)$ and $u_k(\alpha)$ vectors for the α^4 profiling used in § 5. The values of γ and α_0 are the same as in figures 2 and 3. The results displayed are for the case of 48 discrete data points. The angular range, of course, is necessarily restricted to the angle corresponding to the second zero of the Fraunhofer diffraction pattern. As expected the solution-space functions are now much more weighted to the small particle sizes, and are generally smoother. The data-space functions on the other hand are broader, reflecting the increased contribution of the smaller particles.

7. Discussion

The lack of approach to the limit found in § 5 needs further clarification. One possible explanation would be to blame the errors due to quadrature in α used in equation (4.8). To this end the results in table 2 were repeated with the same parameters, but performing a four-point trapezoidal integration within each particle size interval. Although the results changed slightly they were in no case different by more than 2%. This is a similar result to the effect of discrete sampling in the data space shown in table 1.

We believe the failure to approach the limit is due to the inappropriateness of the Fraunhofer approximation for particles in these ranges of optical properties. As mentioned in § 1, the Fraunhofer approximation is derived in a separate way, by considering diffraction by an aperture. A particle will not approximate an aperture unless, possibly, it has infinite imaginary refractive index. Van der Hulst [28] investigated the limit $\alpha \rightarrow \infty$ of the Mie functions. He showed that for $\alpha \gg 1$ the scattered-light intensity contains two separate parts, the first an exact agreement to the Fraunhofer approximation and independent of the particle type, and the second dependent on the particle optical properties, which describes the reflected and refracted rays. Several authors have compared Fraunhofer and Mie functions with reference to this observation [13, 29].

It would be more appropriate to compare Mie functions to such ‘Mie-corrected’ Fraunhofer approximations. We hope to return to this topic in a separate publication.

8. Conclusions

A method for finding the singular system of the Mie scattering kernel for continuous data over all angles has been given. It is based on a result for the spherical harmonic expansion of the kernel. This technique provides a limit to the system obtained using discrete data. In all cases it was found that the use of discrete intervals resulted in slightly reducing the information content of the kernel, in a monotonic fashion with increasing interval size. These conclusions are certainly to be expected, although are necessarily based on a limited set of numerical trials.

An attempt was made to find the Fraunhofer kernel as a large-particle limit of the Mie case. The singular values of the Mie kernel for different ranges of support and discrete data were compared with those of the Fraunhofer kernel for the same discrete data values. It was not possible to approach the Fraunhofer limit despite considering size

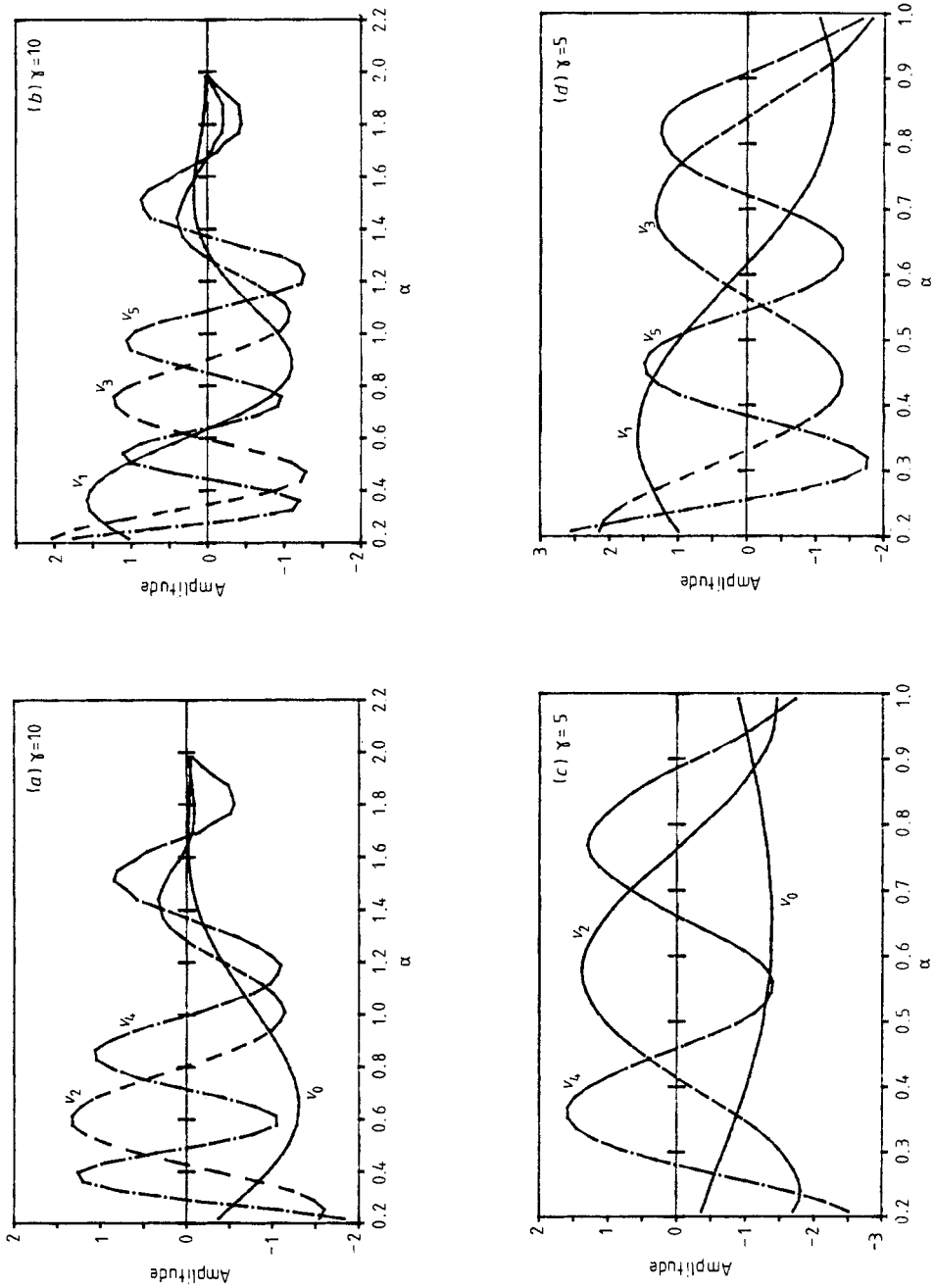


Figure 4. The first six singular vectors v_0, \dots, v_5 in solution space for the α^4 -weighted Mie kernel $\mathcal{X}_{48}[f; \alpha^4]$ (equation (4.1)) for the same parameters as in figure 2.

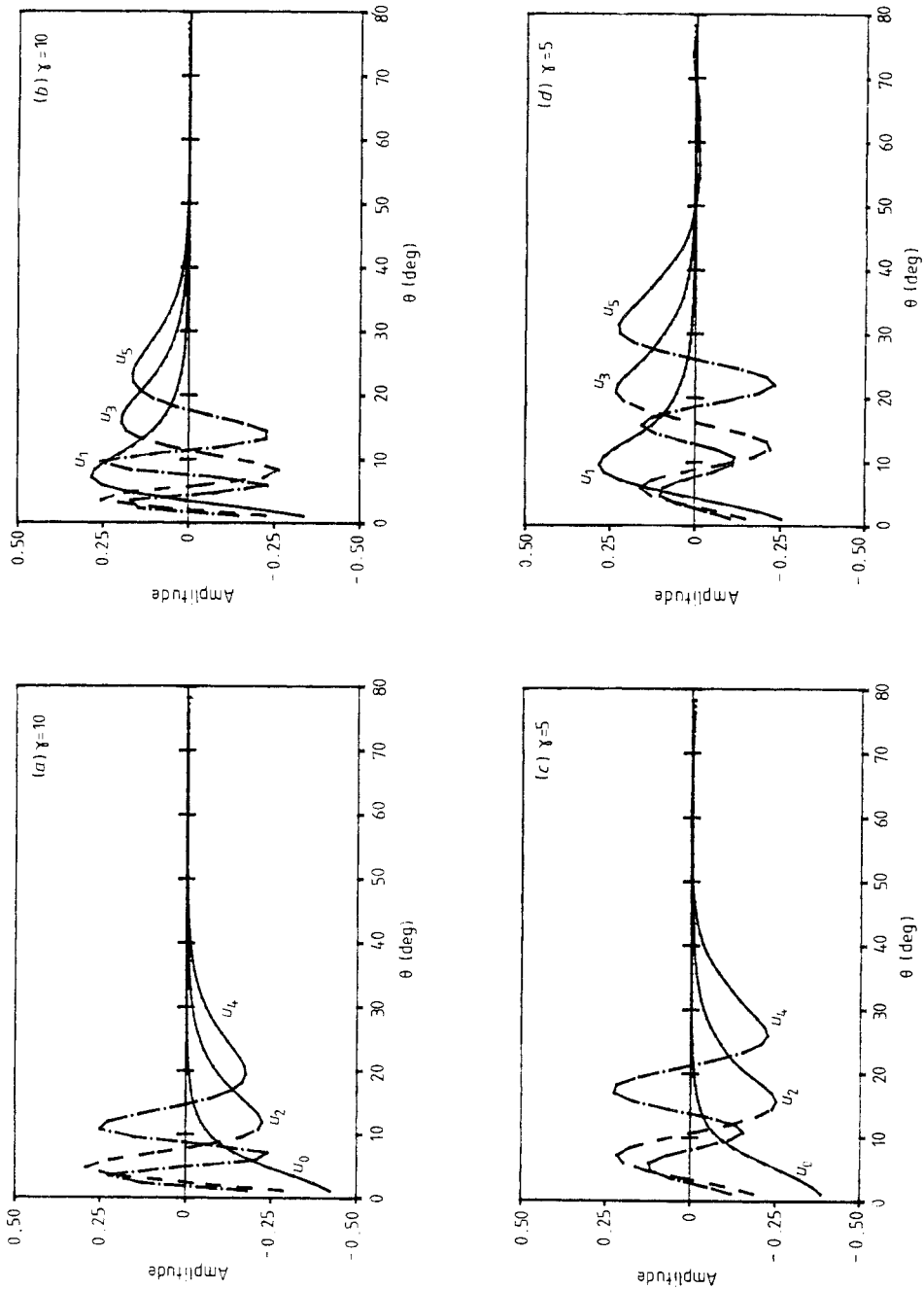


Figure 5. The first six singular vectors u_0, \dots, u_5 in data space for the α^4 -weighted Mike kernel $\mathcal{X}_{\alpha^4}[f; \alpha^4]$ (equation (4.1)) for the same parameters as in figure 3.

parameter ranges normally considered well within the Fraunhofer region ($\alpha > 50$). We believe this lack of approach to the limit is caused by the inapplicability of the Fraunhofer approximation of particles of low imaginary refractive index.

Lastly we note that inversion of scattering data in the Mie region is very sensitive to the choice of support, and to the range of the data. Most inversion schemes attempt to use maximum *a priori* knowledge in this respect. In a subsequent paper we will report on test inversions and regularisation techniques.

Acknowledgments

This work was supported by the SERC, the Wellcome Trust, and Hamamatsu Photonics KK. We gratefully acknowledge the suggestions of Professor E R Pike of King’s College London. We would like to thank M Wylezińska for reading the manuscript.

Appendix. Method for evaluating the Legendre transform of the Mie scattering kernel

For the Mie kernel defined by equation (2.9), we seek the Legendre transform defined by equation (3.10). We will use:

$$F_{n,m}(\mu) = \pi_n(\mu)\pi_m(\mu) + \tau_n(\mu)\tau_m(\mu)$$

$$G_{n,m}(\mu) = \pi_n(\mu)\tau_m(\mu) + \tau_n(\mu)\pi_m(\mu)$$

where π and τ are defined by equations (2.7) and (2.8). Then let \mathcal{L} be the Legendre differential operator

$$\mathcal{L}[f(\mu)] = \frac{d}{d\mu} (1 - \mu^2) \frac{d}{d\mu} [f(\mu)]. \tag{A1}$$

Then the associated Legendre polynomial $P_j^k(\mu)$ satisfies the associated Legendre equation:

$$\mathcal{L}[P_j^k(\mu)] = \left(\lambda_j + \frac{k^2}{(1 - \mu^2)} \right) P_j^k(\mu) \tag{A2}$$

where λ_j is the eigenvalue of the ordinary Legendre equation ($k = 0$) given by $\lambda_j = -j(j + 1)$.

In the Mie kernel, with $k = 1$, we have

$$F_{n,m}(\mu) = \frac{1}{2}[\mathcal{L} - (\lambda_n + \lambda_m)]P_n^1 P_m^1 \tag{A3}$$

$$G_{n,m}(\mu) = \frac{d}{d\mu} [P_m^1 P_n^1]. \tag{A4}$$

Thus substituting into (3.10) we obtain

$$\bar{K}_L(j, \alpha) = \frac{1}{2\alpha^2} \sum_{n,m}^{N_{\max}} \frac{(2n + 1)(2m + 1)}{\lambda_n \lambda_m}$$

$$\times \int_{-1}^1 P_j^0(\mu) \left(A_{m,n} \frac{1}{2}[\mathcal{L} - (\lambda_n + \lambda_m)] + B_{n,m} \frac{d}{d\mu} \right) P_m^1(\mu) P_n^1(\mu) d\mu. \tag{A5}$$

Since \mathcal{L} is self-adjoint we have $\int_{-1}^1 f \mathcal{L} g = \int_{-1}^1 g \mathcal{L} f$, and therefore we obtain

$$\begin{aligned} \bar{K}_L(j, \alpha) &= \frac{1}{2\alpha^2} \sum_{n,m}^{N_{\max}} \frac{(2n+1)(2m+1)}{\lambda_n \lambda_m} \\ &\times \int_{-1}^1 A_{m,n} \frac{1}{2} [\lambda_j - (\lambda_n + \lambda_m)] P_j^0 P_m^1 P_n^1 - B_{n,m} \left[\frac{d}{d\mu} P_j^0 \right] P_m^1 P_n^1 d\mu \end{aligned} \tag{A6}$$

where we have used integration by parts and the fact that $P_j^k(1) = P_j^k(-1) = 0 \forall k \neq 0$.

The first term in equation (A6) is the integral of three associated Legendre polynomials. This is given straightforwardly by the application of the Clebsh–Gordan coefficients (also called the Wigner, or 3- j coefficients) familiar in quantum mechanics,

$$\begin{aligned} \int_{-1}^1 P_j^k(\mu) P_m^l(\mu) P_n^p(\mu) d\mu &= \left(\frac{(1+m)!(j+n)!}{(1-m)!(j-n)!} \right)^{1/2} \\ &\times C(j, m, n; k, l, -p) C(j, m, n; 0, 0, 0) \left(\frac{(k+p)!}{(k-p)!} \right) \end{aligned} \tag{A7}$$

where $p = m + n$. The Clebsh–Gordan (CG) coefficients arise naturally from consideration of the tensor product of irreducible representations of the Lie group SU(2) of 3D rotation in space [26, 27]. They may be given explicitly by a variety of formulae, such as

$$\begin{aligned} C(j, m, n; k, l, p) &= (-1)^{2j-m+p} \\ &\times \left(\frac{(j+m-n)!(n+j-m)!(m+n-j)!(n+p)!(n-p)!}{(j+m+n+l)!(j+k)!(j-k)!(m+l)!(m-l)!} \right)^{1/2} \\ &\times \sum_s (-1)^s \frac{(j+n-l-s)!(m+l+s)!}{s!(n+p-s)!(s+m-j-p)!(n-m+j-s)!} \end{aligned} \tag{A8}$$

where the summation is understood to be over all values of s such that none of the factorial functions have negative argument. In addition they satisfy many symmetry and recursion formulae. Since only $2N_{\max}$ terms are included, the CG coefficients can be precomputed up to $j = 2N_{\max}$, $m = N_{\max}$, $n = N_{\max}$.

The second term in (A6) involves the derivative $(P_j^0)'$. This may be obtained by considering the recurrence relation

$$(2j+1)P_j^0 = (P_{j+1}^0)' - (P_{j-1}^0)' \tag{A9}$$

to generate an expansion

$$(P_j^0)' = \begin{cases} \sum_{k=0}^{(j-1)/2} (4k+1)P_{2k}^0 & j \text{ odd} \\ \sum_{k=0}^{j/2-1} (4k+3)P_{2k+1}^0 & j \text{ even} \end{cases} \tag{A10}$$

which allows the integral to be expressed as a summation over terms given by equation (A7). Substituting (A7) and (A10) into (A6) gives equation (3.11) in the text.

References

[1] Mie G 1908 Beitrage zur Optik trüber Median spezial kolloidaler Metallösungen *Ann. Phys., Lpz.* **25** 377–445
 [2] Kerker M 1969 *The Scattering of Light and other Electromagnetic Radiation* (New York: Academic Press)

- [3] Bohren G F and Huffman D R 1983 *Absorption and Scattering of Light by Small Particles* (New York: Wiley)
- [4] Bertero M and Pike E R 1983 Particle size distribution from Fraunhofer diffraction I: an analytical eigenfunction approach *Opt. Acta* **30** 1043–9
- [5] Bertero M, Boccacci P and Pike E R 1985 Particle size distribution from Fraunhofer diffraction: the singular value spectrum *Inverse Problems* **1** 111–26
- [6] McWhirter J G and Pike E R 1978 On the numerical inversion of the Laplace transform and similar Fredholm integral equations of the first kind *J. Phys. A: Math. Gen.* **11** 1729–45
- [7] Twomey S and Howell H B 1967 Some aspects of the optical estimation of microstructure in fog and cloud *Appl. Opt.* **6** 2125–31
- [8] Phillips D L 1962 A technique for the numerical solution of certain integral equations of the first kind *J. ACM* **9** 84–97
- [9] Twomey S 1963 On the numerical solution of Fredholm integral equations of the first kind by the inversion of the linear system produced by quadrature *J. ACM* **10** 97–101
- [10] Alger T W 1979 Polydisperse particle size distribution function determined from intensity profile of angularly scattered light *Appl. Opt.* **18** 3494–500
- [11] Ben-David A and Herman B M 1985 Method for determining particle size distributions by nonlinear inversion of backscattered radiation *Appl. Opt.* **25** 1037–42
- [12] Dave J V 1971 Determination of size distribution of spherical polydispersions using scattered radiation data *Appl. Opt.* **10** 2035–44
- [13] Fymat A L and Mease K D 1981 Mie forward scattering: improved semiempirical approximation with application to particle size distribution inversion *Appl. Opt.* **20** 194–8
- [14] O'Neill N T and Miller J R 1982 Constrained linear inversion of optical scattering data for particle size spectra: an approach angular optimization *Appl. Opt.* **21** 1231–5
- [15] Santer R and Herman M 1983 Particle size distributions from forward scattered light using the Chahine inversion scheme *Appl. Opt.* **22** 2294–301
- [16] Schrader H W and Eisert W G 1986 High resolution particle sizing using the combination of time of flight and light scattering measurements *Appl. Opt.* **25** 4396–401
- [17] Westwater E R and Cohen A 1973 Application of Backus–Gilbert inversion techniques to determination of aerosol size distributions from optical scattering measurements *Appl. Opt.* **12** 1340–8
- [18] Hanson R J 1971 A numerical method solving Fredholm integral equations of the first kind using singular values *SIAM J. Num. Anal.* **8** 616–22
- [19] Varah J M 1973 On the numerical solution of ill-conditioned linear systems with applications to ill-posed problems *SIAM J. Num. Anal.* **10** 257–67
- [20] Tikhonov A N and Arsenin V Y 1977 *Solutions of Ill-Posed Problems* (Washington, DC: Winston)
- [21] Viera G and Box M A 1985 Information content analysis of aerosol remote-sensing experiments using analytical eigenfunction theory: anomalous diffraction approximation *Appl. Opt.* **24** 4525–33
- [22] Fahlen T S and Bryant H C 1968 Optical backscattering from single water droplets, *J. Opt. Soc. Am.* **58** 304–10
- [23] Chylek P, Kiehl J T and Ko M K W 1978 Narrow resonance structure in the Mie scattering characteristics *Appl. Opt.* **17** 3019–21
- [24] Sneddon I N 1972 *The Use of Integral Transforms* (New York: McGraw-Hill)
- [25] Arridge S R 1989 A note on the spherical harmonic expansion of the Mie scattering kernel *J. Mod. Opt.* **36** 685–92
- [26] Talman J D 1968 *Special Functions: a Group Theoretic Approach* (New York: Benjamin)
- [27] Wawrzyńczyk A 1984 *Group Representation and Special Functions* (Warsaw: Polish Scientific Publishers)
- [28] van der Hulst H C 1957 *Light Scattering by Small Particles* (New York: Wiley)
- [29] Ungut A, Grehan G and Gouesbet G 1981 Comparisons between geometrical optics and Lorenz–Mie theory *Appl. Opt.* **20** 2911–8